Materials Research Proceedings 28 (2023) 285-292 https://doi.org/10.21741/9781644902479-31

A unit-cell mesoscale modelling of biaxial non-crimp-fabric based on a hyperelastic approach

ZHENG Ruochen[1,a *], SCHÄFER Bastian[2,b], PLATZER Auriane[1,c], COLMARS Julien[1,d], NAOUAR Naim[1,e] and BOISSE Philippe[1,f]

[1]Univ Lyon, INSA-Lyon, CNRS UMR5259, LaMCoS, F-69621, France

[2]Karlsruhe Institute of Technology (KIT), Institute of Vehicle System Technology (FAST), Karlsruhe, Germany

[a]ruochen.zheng@insa-lyon.fr, [b]bastian.schaefer@kit.edu, [c]auriane.platzer@insa-lyon.fr, [d]juline.colmars@insa-lyon.fr, [e]naim.naouar@insa-lyon.fr, [f]philippe.boisse@insa-lyon.fr

Keywords: Biaxial NCF, Hyperelastic, Meso-Scale Model, Unit Cell

Abstract. Understanding the mechanical properties of carbon fiber reinforcements is necessary for the simulation of forming processes. A unit-cell mesoscopic model provides a tool to implement virtual material characterizations which can be served as an input for macroscopic modelling, avoiding complex experimental tests and significantly reducing calculation time. Meanwhile, the occurrence of some local defects during the forming process, such as the gapping, would be easier to be detected through a mesoscopic approach. In this research, a novel mesoscale model for biaxial non-crimp fabric is developed based on the geometry measured from the results of X-ray tomography. A hyperelastic constitutive law is applied to the fiber yarns which are considered as a continuous medium. One type of unit-cell model is chosen and validated through a comparison with experimental tests and its in-plane shear behavior is studied.

Introduction

Biaxial non-crimp fabric (Bi-NCF) is increasingly used nowadays due to its higher lightweight potential and lower cost of manufacturing in various areas such as aeronautics and automotive [1]. Unlike a woven fabric, its fiber yarns in both directions are straight without any undulations and each of them is bound with a stitching loop along a specific direction that can be adapted to a desired formability [2]. Different stitching patterns strongly effect the final mechanical properties and drapability of the Bi-NCF [3,4]. Some optical observation methods were carried out by many researchers in order to better understand the internal geometry of NCFs, which is a critical step for the mesoscopic modelling [5,6].

In the literature, macroscopic approaches are commonly used to predict the forming behavior of fibrous reinforcements [7-10]. However, such an approach may encounter difficulties when predicting some local defects, such as the gapping which occurs when the two adjacent yarns move away from each other and leave an empty zone without fibers. These gapping defects are often detected through a numerical result of the in-plane transverse strain at this macroscale [7,11]. Furthermore, yarn-yarn and also stitch-yarn slippage, which usually occur in non-crimp-fabrics, is hard to be seen via a macroscopic continuum approach. An alternative is using microscopic approaches, where each filament of the fiber yarn is modelled by beam or solid elements. This micro-model is realistic but complex and time-consuming. Therefore, mesoscopic approaches are much more used on the Biaxial-NCF or even UD-NCF [12,13].

Mesoscopic modelling considers each fibrous yarn as a solid medium and the surrounding stitches are modelled by finite beam or bar elements. The contact behavior between the stitches and yarns are considered as well. Therefore, the local deformation of NCFs, such as the yarn's compression, the slippage between yarns and stitches, as well as the development of gap, is visible

at this scale. This work aims to develop and introduce a unit cell mesoscopic model in commercial software Abaqus, on which virtual material characterization can be conducted and different stitching pattern can be analyzed.

Unit Cell Mesoscopic Model

In this research, a $0^{\circ}/90^{\circ}$ carbon fiber biaxial NCF with a polyester tricot stitching is selected. The two layers are bound together during the production process with loop formation in the warp direction. The fiber yarns in the warp direction which are characterized with a "Z" stitching pattern are shown in Fig. 1a, and the weft fiber yarns are shown in Fig. 1b. Its areal weight is 600 g/m^2.

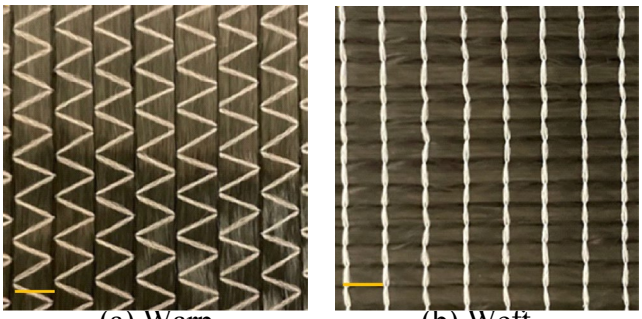

(a) Warp (b) Weft

Fig. 1. carbon biaxial non-crimp fabric architecture.

In order to better understand its internal geometry, an X-ray tomography was firstly carried out, as shown in Fig. 2a. Several geometrical parameters, such as the width and thickness of weft and warp fiber yarns, the knitting position (where the stitch passes through the two layers of fiber yarns), the initial gap between fiber yarns, were measured to serve as input for the mesoscopic model.

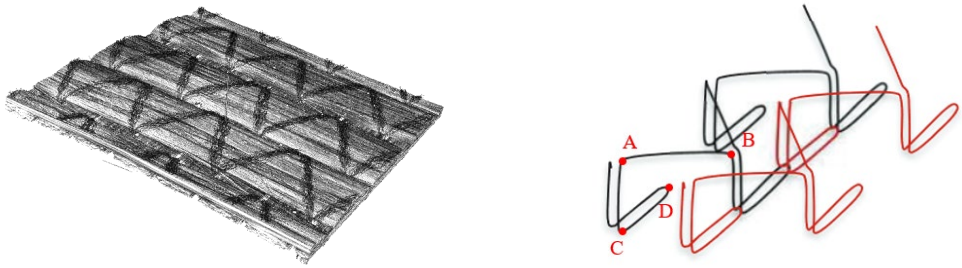

(a) (b)

Fig. 2. Geometry of NCF (a) X-ray tomography (b) tricot stitching pattern schema [24].

The cross-section shape of the fiber yarns was assumed to be circular, flat, elliptic or biconvex in several researches [14-16]. In this study, the yarn's section was built as a half elliptical shape and the yarn is considered to be straight as an ideal initial configuration. The tricot stitch pattern is shown in Fig. 2b. It is complex to observe the stitch geometry since some of stitch yarns are hidden between the fiber yarns. Researchers use tracer fiber techniques to extract the stitching path [6] and define mathematical equations to describe these explicitly [17]. For an example of stitching loop shown in Fig. 2b, the A, B, C and D points are the knitting position where the stitch yarn goes through the two layers of fiber yarn. Their locations can be confirmed from tomography results. From A to B and C to D, two elliptical equations are respectively used to describe the stitch yarn to wrap around the weft and wrap yarn. From A to C is a straight line to describe the piercing stitch. Through repeating these steps, the whole stitching pattern can be generated. After assembling the fiber yarns and stitches, a simulation of the shrinkage of the stitch is carried out in order to tighten the initial loose structure and realize the interaction between the yarn systems [18].

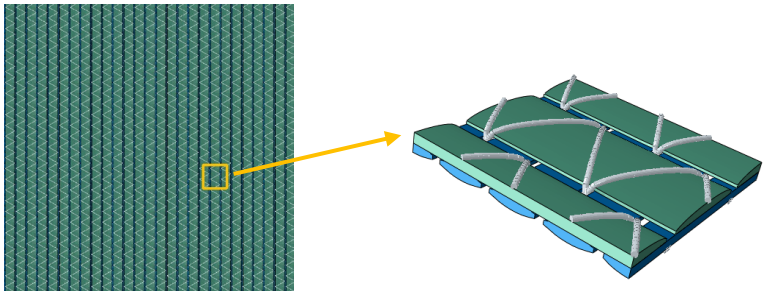

Fig. 3. Modeling of biaxial NCF.

One selected type of unit cell model is shown in Fig. 3. It has the smallest size to contain at least one entire stitching loop and is able to represent the entire mechanical properties of the NCF. A half yarn position is chosen as this model's boundary rather than the gap position because it will not break the stitching loop connection (which is point D in Fig. 2b). Otherwise the separation of stitches may happen which requires additional boundary conditions.

Boundary Conditions and Periodicities

It is assumed that the biaxial NCF is a periodic medium if the internal slippage is neglected and in order to guarantee this periodicity, appropriate kinematic boundary conditions need to be imposed on the unit cell so that it can represent the mechanical property of entire fabric [19]. The displacement field $\underline{\varphi}(\underline{X})$ of the structure can be split into two parts, as shown in Fig. 4: the macroscopic displacement field $\underline{\varphi_m}(\underline{X})$ which is known since it is the input of the simulation and the periodic local displacement $\underline{w}(\underline{X})$ which is unknown [20,21].

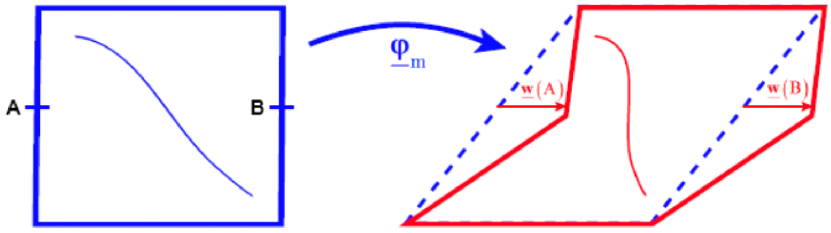

Fig. 4. Initial and deformed periodic structure, displacement field.

This can be expressed as:

$$\underline{\varphi}(\underline{X}) = \underline{\varphi_m}(\underline{X}) + \underline{w}(\underline{X}) \tag{1}$$

To ensure the periodicities, it is necessary to make sure that the local displacements of two opposite sides $\underline{X^+}$ and $\underline{X^-}$ are equal

$$\underline{w}(\underline{X^+}) = \underline{w}(\underline{X^-}) \tag{2}$$

Then the boundary conditions can be obtained as:

$$\underline{\varphi}(\underline{X^+}) - \underline{\varphi}(\underline{X^-}) = \underline{\varphi_m}(\underline{X^+}) - \underline{\varphi_m}(\underline{X^-}) \tag{3}$$

Materials Research Proceedings 28 (2023) 285-292 https://doi.org/10.21741/9781644902479-31

Mechanical Behavior of the Fiber Yarn and Stitch

In this study, the polyester stitch was modelled by two-node beam elements and was considered as a linear elastic material. A traction test was carried out to measure its tensile stiffness. A hyperelastic constitutive law which had been proposed by A. Charmetant [22] was used for the carbon fiber yarn.

Hyperelastic constitutive law.

The fiber yarn is specific as it contains thousands of filaments of carbon fibers, giving it high tensile stiffness and relatively low shear stiffness. From the cross-sectional images at the microscopic scale, the two-point covariance, which represents the probability that two points separated by a distance x to belong to the same phase of the fiber, looks similar along the width and thickness of each fiber yarn [20]. Thus, it can be assumed that the spatial distribution of these filaments inside the yarn is isotropic and the fiber yarn is considered to be transverse isotropy. Four deformation modes are used to describe the fiber yarn's behavior, which are the elongation along the fiber direction, the compaction of the cross section, the transverse shear (distortion of the cross section), and the longitudinal shear along the fiber direction, as shown in Fig. 5.

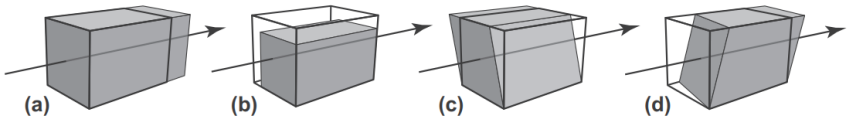

Fig. 5. Four deformation modes of fiber yarn (a) elongation (b) compaction of cross section (c) transverse shear (d) longitudinal shear.

Thus, the deformation gradient tensor, $\underline{F}$, which allows the transformation of fiber yarn from its initial position $\underline{X}$ to its deformed position $\underline{x}$, can be split into four matrixes associated with these four deformation modes.

$$\left[\underline{F}\right] = \left[\underline{\underline{F_{elong}}}\right] \vdots \left[\underline{\underline{F_{comp}}}\right] \vdots \left[\underline{\underline{F_{dist}}}\right] \vdots \left[\underline{\underline{F_{sh}}}\right] \tag{4}$$

The hyperelastic equation defines the material's elastic strain energy potential based on the strain state. Four physically based invariants I_{elong}, I_{comp}, I_{dist}, I_{sh} are defined as a function of the classical invariants I_1 to I_5 of the right Cauchy Green strain tensor $\underline{\underline{C}}$ and then used to describe these different deformation modes.

These classical invariants are expressed as:

$$I_1 = trace(\underline{\underline{C}}),\ I_2 = \frac{1}{2}(trace\left(\underline{\underline{C}}\right)^2 - trace(\underline{\underline{C}}^2)), I_3 = det(\underline{\underline{C}})$$

$$I_4 = \underline{\underline{C}} : \underline{\underline{M}}, \qquad I_5 = \underline{\underline{C}}^2 : \underline{\underline{M}} \tag{5}$$

where $\underline{\underline{M}}$ is a structural tensor defined by a unit vector of preferred direction $\underline{M}$, i.e. the fiber direction:

$$\underline{\underline{M}} = \underline{M} \otimes \underline{M} \tag{6}$$

The four physically based invariants are introduced in [22] and expressed as:

$$I_{elong} = \frac{1}{2} ln\, ln\, I_4\,,\; I_{comp} = \frac{1}{4} ln\, ln\, (\frac{I_3}{I_4})\,,\; I_{dist} = \frac{1}{2} ln\, ln\, (\frac{I_1 I_4 - I_5}{2\sqrt{I_3 I_4}} + \sqrt{(\frac{I_1 I_4 - I_5}{2\sqrt{I_3 I_4}})^2 - 1})\,,\; I_{sh} = \sqrt{\frac{I_5}{I_4{}^2} - 1} \quad (7)$$

Then, the deformation energy is assumed to be the sum of the energies of these four deformation modes:

$$w(\underline{\underline{F}}) = w_{elong}(I_{elong}) + w_{comp}(I_{comp}) + w_{dist}(I_{dist}) + w_{sh}(I_{sh}) \quad (8)$$

The second Piola-Kirchhoff stress tensor is defined as

$$\underline{\underline{S}} = 2\frac{\partial w}{\partial \underline{\underline{C}}} = 2(\frac{\partial w_{elong}}{\partial I_{elong}}\frac{\partial I_{elong}}{\partial \underline{\underline{C}}} + \frac{\partial w_{comp}}{\partial I_{comp}}\frac{\partial I_{comp}}{\partial \underline{\underline{C}}} + \frac{\partial w_{dist}}{\partial I_{dist}}\frac{\partial I_{dist}}{\partial \underline{\underline{C}}} + \frac{\partial w_{sh}}{\partial I_{sh}}\frac{\partial I_{sh}}{\partial \underline{\underline{C}}}) \quad (9)$$

Experimental tensile tests and compaction tests on woven fabric and single fiber yarn were carried out in several previous researches [22,25]. Since the studied Bi-NCF is also made of carbon fibers, the same material parameters are temporarily used and are shown in Table 1.

Table 1. Parameters of the constitutive model for the yarn.

Deformation mode	Strain energy function	Material parameters
Elongation	$w_{elong}(I_{elong}) = \frac{1}{2} K_{elong} {I_{elong}}^2$	K_{elong}=108500 N
Compaction	$w_{comp}(I_{comp}) = \lvert K_{comp} {I_{comp}}^p \quad 0 \;\; if\; I_{comp} > 0$	K_{comp}=1.25 Mpa $P = 1.84$
Transverse shear	$w_{dist}(I_{dist}) = \frac{1}{2} K_{dist} {I_{dist}}^2$	K_{dist}=0.6Mpa
Longitudinal shear	$w_{sh}(I_{sh}) = \frac{1}{2} K_{sh} {I_{sh}}^2$	K_{sh}=2Mpa

Numerical Study

The virtual tests such as the elongation tests or compaction tests can be done on the unit cell model. In this study, an in-plane shear simulation was carried out to validate this unit cell model through comparing the deformed geometry and the shear force with the experimental results, after assuming that the shear deformation is uniformly distributed. Fig. 6a shows the in-plane shear deformation schema. The nodes at the bottom corner were fixed and the nodes at the top corner were stretched. The unit cell length was 10 mm, and the displacement of the stretched nodes was set up as 5 mm. The deformed configuration of this unit cell is shown in Fig. 6b. During the shear deformation, it can be seen that one segment of stitch is always stretched and another one is compressed. The fiber yarns are also compressed by the tightened stitches. In order to validate the deformed geometry, the yarn's width as well as the gap are measured. They all show a good agreement with the experiments.

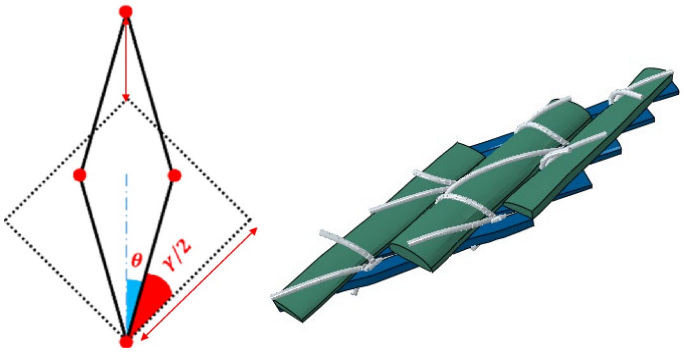

(a) (b)

Fig. 6. (a) Schema of an in-plane shear deformation [26] (b) Deformed unit cell model.

The shear angle during this deformation can be expressed as:

$$\gamma = \frac{\pi}{2} - 2\theta = \frac{\pi}{2} - 2(\frac{\sqrt{2}L+D}{2L}) \quad (10)$$

where L is the unit cell length and D is the displacement.

In order to compare with the experimental results, the reaction force F which is measured at the fixed nodes is normalized by the frame length [23]:

$$F_{nor} = \frac{F \cdot L}{\sqrt{2}L+D} / L \quad (11)$$

The simulation results of normalized shear force and shear angle are shown in Fig. 7, showing a good agreement with the experimental results.

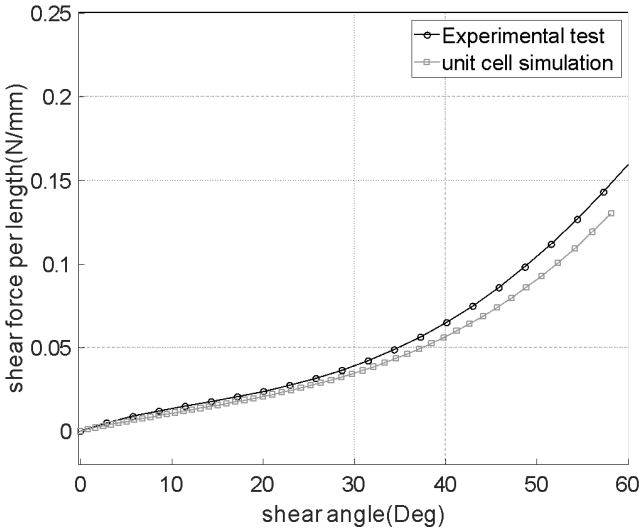

Fig. 7. Shear force normalized vs. shear angle.

Summary

A unit cell mesoscopic finite element model with explicitly described geometry of fiber yarns and stitches is proposed in this study. This model is validated through an in-plane shear simulation, where the shear force and the deformed geometry are in good agreements with experimental results. It shows that this model is able to conduct virtual material characterization and significantly reduce the necessary amount of experimental tests. Furthermore, the geometry of stitches and yarn's section can be easily adjusted which allows for the analysis of different stitching patterns, with the opportunity to develop tailored NCFs with optimized deformation behavior for specific applications.

The hyperelastic constitutive law that is applied on carbon fiber yarns in this study does not consider the bending behavior which is necessary when conducting forming simulation and analyzing gapping defect. The generalized continua approach is needed to be developed and implemented in the future work.

Acknowledgement

This work is funded by the French National Research Agency (ANR) and the Deutsche Forschungsgemeinschaft (DFG, German Research Foundation) in the collaborative project "Composite forming simulation for non-crimp fabrics based on generalized continuum approaches".

References

[1] P. Middendorf, C. Metzner, Aerospace applications of non-crimp fabric composites, in: Stepan V. Lomov (Eds.), Non-Crimp Fabric Composites, Woodhead Publishing (2011) 441-449. https://doi.org/10.1533/9780857092533.4.441

[2] A. Schnabel, T. Gries, Production of non-crimp fabrics for composites, in: Stepan V. Lomov (Eds.), Non-Crimp Fabric Composites, Woodhead Publishing (2011) 3-41. https://doi.org/10.1533/9780857092533.1.3

[3] S. Bel, P. Boisse, F. Dumont, Analyses of the Deformation Mechanisms of Non-Crimp Fabric Composite Reinforcements during Preforming, Appl. Compos. Mater. 19 (2012) 513-528. https://doi.org/10.1007/s10443-011-9207-x

[4] H. Krieger, T. Gries, S. E. Stapleton, Shear and drape behavior of non-crimp fabrics based on stitching geometry, Int. J. Mater. Form. 11 (2018) 593-605. https://doi.org/10.1007/s12289-017-1368-1

[5] H. Yin, Q. Li, L. Iannucci, Meso-scale Finite Element (FE) modelling of biaxial carbon fibre non-crimp-fabric (NCF) based composites under uniaxial tension and in-plane shear, Compos. Struct. 290 (2022) 115538. https://doi.org/10.1016/j.compstruct.2022.115538

[6] W. Wu, W. Li, Parametric modeling based on the real geometry of glass fiber unidirectional non-crimp fabric, Text. Res. J. 89 (2019) 3949-3959. https://doi.org/10.1177/0040517518824846

[7] J. Schirmaier, D. Dörr, F. Henning, and L. Kärger, A macroscopic approach to simulate the forming behaviour of stitched unidirectional non-crimp fabrics (UD-NCF), Compos. Part A 102 (2017) 322-335. http://dx.doi.org/10.1016/j.compositesa.2017.08.009

[8] B. Chen, J. Colmars, N. Naouar, N, P. Boisse, P, A hypoelastic stress resultant shell approach for simulations of textile composite reinforcement forming. Compos. Part A Appl. Sci. Manuf. 149 (2021) 106558. https://doi.org/10.1016/J.COMPOSITESA.2021.106558

[9] L. Kärger, S. Galkin, E. Kunze, M. Gude, B. Schäfer, Prediction of forming effects in UD-NCF by macroscopic forming simulation - Capabilities and limitations. Paper presented at ESAFORM 2021, 24th International Conference on Material Forming, Liège, Belgique. https://doi.org/10.25518/esaform21.355

[10] P. Boisse, N. Hamila, E. Vidal-Sallé, F. Dumont, Simulation of wrinkling during textile composite reinforcement forming. Influence of tensile, in-plane shear and bending stiffnesses, Compos. Sci. Technol. 71 (2011) 683-692. https://doi.org/10.1016/j.compscitech.2011.01.011

[11] S. Galkin, E. Kunze, L. Kärger, R. Böhm, M. Gude, Experimental and Numerical Determination of the Local Fiber Volume Content of Unidirectional Non-Crimp Fabrics with Forming Effects, J. Compos. Sci. 3 (2019) 19. https://doi.org/10.3390/jcs3010019

[12] G. Creech, A. K. Pickett, Meso-modelling of Non-Crimp Fabric composites for coupled drape and failure analysis. J. Mater. Sci. 41 (2006) 6725-6736. https://doi.org/ 10.1007/s10853-006-0213-6

[13] L. Li, Y. Zhao, H. Vuong, Y. Chen, J. Yang, Y. Duan, In-plane shear investigation of biaxial carbon non-crimp fabrics with experimental tests and finite element modeling, Mater. Des. 63 (2014) 757-765. https://doi.org/10.1016/j.matdes.2014.07.007

[14] S.V. Lomov, G. Huysmans, Y. Luo, R.S. Parnas, A. Prodromou, I. Verpoest, F.R. Phelan, Textile composites: modelling strategies, Compos. Part A 32 (2001) 1379-1394. https://doi.org/10.1016/S1359-835X(01)00038-0

[15] J. Whitcomb, X. Tang, Effective Moduli of Woven Composites, J. Compos. Mater. 35 (2001) 2127-2144. http://doi.org/10.1177/002199801772661380

[16] D. Goyal, X. Tang, J. Whitcomb, A. D. Kelkar, Effect of various parameters on effective engineering properties of 2 × 2 braided composites. Mech. Compos. Mater. Struct. 12 (2005) 113-128. https://doi.org/10.1080/15376490490493998

[17] S.V. Lomov, E.B. Belov, T. Bischoff, S.B. Ghosh, T. Truong Chi, I. Verpoest, Carbon composites based on multiaxial multiply stitched preforms. Part 1. Geometry of the preform, Compos. Part A 33 (2002) 1171-1183. https://doi.org/10.1016/S1359-835X(02)00090-8
[18] M. Q. Pham, E. Wendt, E. Häntzsche, T. Gereke, C. Cherif, Numerical modeling of the mechanical behavior of textile structures on the meso-scale for forming process simulations of composite 3D preforms, Engin. Reports 4 (2022) 12348. https://doi.org/10.1002/eng2.12348
[19] C. Miehe, J. Dettmar, A framework for micro-macro transitions in periodic particle aggregates of granular materials, Comput. Methods Appl. Mech. Engin. 193 (2004) 225-256. https://doi.org/10.1016/j.cma.2003.10.004
[20] P. Badel, E. Vidal-Sallé, E. Maire, P. Boisse, Simulation and tomography analysis of textile composite reinforcement deformation at the mesoscopic scale, Compos. Sci. Technol. 68 (2008) 2433-2440. https://doi.org/10.1016/j.compscitech.2008.04.038
[21] P. Badel, E. Vidal-Sallé, P. Boisse, Computational determination of in-plane shear mechanical behaviour of textile composite reinforcements, Computat. Mater. Sci. 40 (2007) 439-448. https://doi.org/10.1016/j.commatsci.2007.01.022
[22] A. Charmetant, E. Vidal-Sallé, P. Boisse, Hyperelastic modelling for mesoscopic analyses of composite reinforcements, Compos. Sci. Technol. 71 (2011) 1623-1631. https://doi.org/10.1016/j.compscitech.2011.07.004
[23] J. Cao, R. Akkerman, P. Boisse, J. Chen, H.S. Cheng, E.F. de Graaf, J.L. Gorczyca, P. Harrison, G. Hivet, J. Launay, W. Lee, L. Liu, S.V. Lomov, A. Long, E. de Luycker, F. Morestin, J. Padvoiskis, X.Q. Peng, J. Sherwood, Tz. Stoilova, X.M. Tao, I. Verpoest, A. Willems, J. Wiggers, T.X. Yu, B. Zhu, Characterization of mechanical behavior of woven fabrics: Experimental methods and benchmark results, Compos. Part A Appl. Sci. Manuf. 39 (2008) 1037-1053. https://doi.org/10.1016/j.compositesa.2008.02.016
[24] Q. Steer, J. Colmars, P. Boisse, Modeling of tricot stitch non crimp fabric in forming simulations, AIP Conference Proceedings 2113 (2019) 020004.https://doi.org/10.1063/1.5112509
[25] A. Iwata, T. Inoue, N. Naouar, P. Boisse, S. V. Lomov, Coupled meso-macro simulation of woven fabric local deformation during draping, Compos. Part A 118 (2019) 267-280. https://doi.org/10.1016/j.compositesa.2019.01.004
[26] A. Habboush, N. Sanbhal, H. Shao, J. Jiang, N. Chen, Characterization and Analysis of In-Plane Shear Behavior of Glass Warp-Knitted Non-Crimp Fabrics Based on Picture Frame Method, Materials 11 (2018) 1550. https://doi.org/10.3390/ma11091550